# LncRNA HOTAIR Interaction With WTAP Promotes m$^6$A Methyltransferase Complex Assembly and Posterior Capsule Opacification Formation by Increasing THBS1

Xi Chen,[1,2] Chenshuang Li,[1] Jiankui Li,[3] Zaoxia Guo,[1] Siqi Zhang,[1] Chenjun Guo,[4] and Hong Yan[1,2]

[1]Shaanxi Eye Hospital, Xi'an People's Hospital (Xi'an Fourth Hospital), Affiliated People's Hospital of Northwest University, Xi'an, Shaanxi, China
[2]Xi'an Key Laboratory of Stem Cell and Regenerative Medicine, Institute of Medical Research, Northwestern Polytechnical University, Xi'an, Shaanxi, China
[3]Department of Gynecology & Obstetrics, The 960th Hospital of PLA, Jinan, Shandong, China
[4]Department of Ophthalmology, Tangdu Hospital, Air Force Medical University, Xi'an, Shaanxi, China

Correspondence: Hong Yan, Shaanxi Eye Hospital, Xi'an People's Hospital (Xi'an Fourth Hospital), Northwest University, 21 Jiefang Rd., Xi'an, Shaanxi 710004, China; yan2128ts@med.nwu.edu.cn.

**Received:** January 21, 2025
**Accepted:** April 15, 2025
**Published:** May 9, 2025

Citation: Chen X, Li C, Li J, et al. LncRNA HOTAIR interaction with WTAP promotes m$^6$A methyltransferase complex assembly and posterior capsule opacification formation by increasing THBS1. *Invest Ophthalmol Vis Sci.* 2025;66(5):20. https://doi.org/10.1167/iovs.66.5.20

**Purpose.** To explore the role of long non-coding RNAs (lncRNAs) and $N^6$-methyladenosine (m$^6$A) in posterior capsule opacification (PCO) and their underlying mechanisms.

**Methods.** The localization of lncRNAs and proteins was analyzed using fluorescence in situ hybridization and immunofluorescence staining. RNA m$^6$A quantification, RNA immunoprecipitation, co-immunoprecipitation, MeRIP-seq, MeRIP-qPCR, western blotting, wound healing, and Transwell assays were applied to elucidate the underlying mechanisms.

**Results.** The levels of lncRNA HOX transcript antisense intergenic RNA (HOTAIR) and m$^6$A methylation increased significantly during epithelial–mesenchymal transition (EMT) in lens epithelial cells (LECs). HOTAIR promoted EMT and m$^6$A methyltransferase activity but had no effect on methyltransferase activity and was not modified by m$^6$A. Nevertheless, HOTAIR interacted with WT1-associated protein (WTAP), a key m$^6$A writer protein, facilitating WTAP-mediated recruitment of METTL3–METTL14 heterodimers and enhancing m$^6$A modification. The HOTAIR/WTAP complex elevated m$^6$A levels, thrombospondin 1 (THBS1) expression, and EMT in LECs.

**Conclusions.** LncRNA HOTAIR enhances the assembly of the WTAP/METTL3/METTL14 complex and promotes EMT in LECs by upregulating m$^6$A modification and THBS1 expression. Targeting the HOTAIR/WTAP/THBS1 pathway may prevent or treat PCO.

Keywords: lncRNA HOTAIR, epithelial–mesenchymal transition, $N^6$-methyladenosine, thrombospondin 1, posterior capsule opacification

Cataracts are the leading cause of blindness worldwide and are primarily treated with surgery.[1] Posterior capsule opacification (PCO), a delayed complication,[2] affects 30% of adults[3] and nearly all children post-surgery, impairing their vision.[4] Neodymium-doped yttrium aluminum garnet (Nd:YAG) capsulotomy, the sole treatment, can cause intraocular lens misalignment, retinal detachment, and macular edema.[5,6] Understanding PCO pathogenesis and identifying preventive strategies are crucial. Postoperative wound healing triggers epithelial–mesenchymal transition (EMT) in residual lens epithelial cells (LECs), driving fibrotic PCO,[7,8] although its molecular mechanisms remain unclear.

$N^6$-methyladenosine (m$^6$A), the most common post-transcriptional modification of polyadenylated messenger RNA (mRNA) and long non-coding RNAs (lncRNAs) in higher eukaryotes, involves methylation and demethylation of RNA adenine.[9,10] This dynamic and reversible process is regulated by three proteases.[11] Methylases, including methyltransferase-like protein 3/14 (METTL3/14) and WT1-associated protein (WTAP), install this modification. WTAP, a key m$^6$A methyltransferase component, recruits the METTL3–METTL14 heterodimer to target mRNAs.[12] Demethylases (FTO and ALKBH5) catalyze the modification for uninstallation, whereas reader proteins (YTHDF1/2/3 and IGF2BP1/2/3) are responsible for recognition.[13] m$^6$A is linked to EMT, with METTL3 maintaining epithelial properties and promoting tumor progression via EMT-related molecules.[14,15] However, its role in EMT regulation in LECs remains unexplored.

LncRNAs are non-coding RNA (ncRNA) transcripts over 200 nucleotides that regulate DNA repair, differentiation, metabolism, and tumor migration and invasion.[16] Several lncRNAs, including MIAT, H19, MALAT1, FEZF1-AS1, and NEAT1, influence eye development and disease,[17–19] LEC functions, and EMT.[20–24] HOX transcript antisense intergenic RNA (HOTAIR), a cancer-related lncRNA,[25] promotes

proliferation and migration via EMT pathways[26] and is upregulated in TGF-$\beta$2–treated LECs,[27] although its mechanism remains unclear. m$^6$A modification affects ncRNA cleavage, transport, stability, and degradation.[10] The function of WTAP is modulated by ncRNAs. Circular RNA (circRNA) 0008399 binds to WTAP to modulate METTL3–METTL14 complex formation, promoting global m$^6$A levels in bladder cancer.[28] circRNA PDE5A inhibits WTAP-dependent m$^6$A methylation of eukaryotic translation initiation factor 3c mRNA.[29] LncRNA PCGEM1 promotes tumor progression via WTAP.[30] However, the regulatory mechanism by which HOTAIR modulates WTAP remains unclear. This study investigates how m$^6$A modification and HOTAIR contribute to PCO.

## Methods

### Animal Models and Cataract Surgery

Animal experiments adhered to the guidelines of the Ethics Committee of Northwestern Polytechnical University (202201022) of China and the ARVO Statement for the Use of Animals in Ophthalmic and Vision Research. Mock cataract surgery[31,32] was performed on a balanced cohort of male and female C57BL/6 mice (10 weeks old) per the National Institutes of Health guidelines that recommend balanced sex representation in animal studies.[33] Mice were euthanized 5 days post-surgery, and lens capsules were collected for subsequent analyses. Eight capsules from eight mice lenses were pooled for individual assays for total protein detection. Six capsules from six mice lenses were pooled for each assay for total RNA extraction. Immunofluorescence assays were performed on five eyes from five mice. All tests were performed in triplicate.

### Cell Culture, Treatment, and Transfection

The human lens epithelial B3 cell line (HLE-B3) was obtained from the American Type Culture Collection (ATCC, Manassas, VA, USA) (Supplementary Fig. S1D). It was cultured in Gibco Minimum Essential Medium (MEM, C11095500BT; Thermo Fisher Scientific, Waltham, MA, USA) with 10% Gibco fetal bovine serum (FBS, 10099-141; Thermo Fisher Scientific) and 50 U/mL penicillin/streptomycin (15140122; Thermo Fisher Scientific), followed by incubation at 37°C with 5% $CO_2$. Cells that reached 70% fusion were starved in FBS-free medium for 12 hours,[34,35] then treated with 0, 5, 10, 15, 20, and 25 ng/mL TGF-$\beta$2 (100-35B; PeproTech, Cranbury, NJ, USA).

Lentivirus-mediated HOTAIR and WTAP overexpression vectors (GeneChem, Shanghai, China) were transfected at a cell density of 50% to 60%. After 8 hours, the transfection medium was replaced with a medium containing 10% FBS. After 72 hours, puromycin was used to select the stable clones. Small interfering RNA (siRNA) sequences for HOTAIR, WTAP, and thrombospondin 1 (THBS1) were designed and synthesized by Hanbio (Shanghai, China) (Supplementary Table S1). siRNA (20 µmol/L) was used to infect cells with Invitrogen Lipofectamine 2000 (11668019; Thermo Fisher Scientific) in Gibco Opti-MEM (31985070; Thermo Fisher Scientific) at a cell density of 50% to 60%. After 6 hours, the cells were supplemented with a medium containing 10% FBS. Transfection efficiency was determined using a fluorescence microscope (Olympus, Tokyo, Japan).

### Cell Counting Kit-8 Assay

A 100-µL cell suspension ($1 \times 10^5$ cells) was seeded into each well of a 96-well plate and cultured in an incubator at 37°C in a 5% $CO_2$ atmosphere. Upon reaching 50% confluency, the culture medium was replaced with different treatments, followed by an additional 48-hour incubation. Subsequently, 10 µL Cell Counting Kit-8 (CCK-8) solution (CK04; Dojindo Laboratories, Kumamoto, Japan) was added to each well, and the cells were incubated for 2 hours. The absorbance was measured at 450 nm using a microplate reader (Spark; Tecan, Zurich, Switzerland).

### 5-Ethynyl-2′-Deoxyuridine Assay

Cells were cultured on coverslips placed in a 24-well plate at at 37°C in a 5% $CO_2$ atmosphere, and, upon reaching 30% to 50% density, the cells were subjected to different treatments and incubated for 48 hours. Then, 10 µM 5-ethynyl-2′-deoxyuridine (EdU) solution (C0071S/C0078S; Beyotime, Shanghai, China) prewarmed at 37°C was added to each well, and the cells were incubated for 6 hours before harvesting. Finally, nuclei were stained with Hoechst 33342, and fluorescent images were acquired using confocal microscopy (Olympus). EdU-positive cells were counted using ImageJ (National Institutes of Health, Bethesda, MD, USA).

### Fluorescence In Situ Hybridization and Immunofluorescence Staining

LncRNA fluorescence in situ hybridization (FISH) was performed using a FISH kit (C10910; RiboBio, Guangzhou, China) according to the manufacturer's instructions. Cells on 24-well coverslips were fixed and permeabilized with PBS containing 4% paraformaldehyde (PFA) and 0.5% Triton X-100 (ST795; Beyotime) at room temperature (RT), washed after 20 minutes, and pre-hybridized at 37°C for 30 minutes. Cy3-labeled probes (20 µmol/L) for lncRNA HOTAIR, U6, or 18S (RiboBio) were added to the hybridization buffer and incubated overnight at 37°C in the dark. Slides were washed three times with 2× saline-sodium citrate (SSC) buffer (0.3-M NaCl and 0.03-M $Na_3$ citrate, pH 7.0), once with 1× SSC, and once with 1× PBS at RT. The air-dried slides were stained with DAPI (RiboBio). U6 and 16S probes served as nuclear internal and cytoplasmic controls, respectively.

For immunofluorescence (IF) staining, cells at 40% density and posterior capsules from mouse eyes were rinsed with PBS, fixed with 4% PFA, and permeabilized with 0.3% Triton X-100 at RT. Blocking buffer, PBS with 5% normal donkey serum (SL050; Solarbio, Beijing, China), was applied for 30 minutes at RT, followed by 12-hour incubation with primary antibodies at 4°C. After washing with PBS (3 × 5 minutes), the secondary antibody was incubated for 90 minutes at RT in the dark, followed by washing with PBS. Nuclei were stained with 4′,6-diamidino-2-phenylindole (DAPI, C1005; Beyotime). Coverslips were treated with an anti-fluorescence quenching solvent, and IF images were acquired using an Olympus confocal microscope with consistent settings. Images were analyzed using the Olympus FV31S-SW Viewer and FV31S-DT software.

### RNA m$^6$A Quantification

Total RNA was isolated from the cells and lens capsules using TRIzol reagent (9108; Takara Bio, Tokyo, Japan). m$^6$A modi-

Investigative Ophthalmology & Visual Science

fication was detected using the EpiQuik m$^6$A RNA Methylation Quantification Kit (Colorimetric) (P-9005; EpiGentek, Farmingdale, NY, USA). A 96-well plate was prepared with 2 µL negative control (NC), 2 µL diluted positive control, and 200 ng RNA in 80 µL of binding solution. Membranes were sequentially incubated with capture and detection antibodies, enhancer solution, and 100 µL developer solution. Signaling was measured at RT for 6 minutes in the dark. Stop solution (100 µL) was added to halt the enzyme reaction within 2 to 15 minutes using a Tecan Spark microplate reader at 450 nm. The manufacturer's formula was used to compute the relative m$^6$A RNA methylation status.

### Quantitative Real-Time-PCR

RNA was extracted from mouse lens capsules and HLE-B3 cells using TRIzol reagent, followed by reverse transcription with PrimeScript RT Reagent Kit (RR820A; Takara Bio). TB Green Premix Ex Taq II (RR036A; Takara Bio) was used to amplify target genes, and data were collected using a QuantStudio 5 Real-Time PCR System (Thermo Fisher Scientific). Glyceraldehyde-3-phosphate dehydrogenase (GAPDH) was the internal control. The analysis included three replicates, and primers (Supplementary Table S2) were obtained from Sangon Biotech (Shanghai, China).

### RNA Immunoprecipitation Assay

The CatRAPID database predicted WTAP–HOTAIR interactions, which were validated using the EZ-Magna RIP RNA-Binding Protein Immunoprecipitation Kit (17-701; Merck Millipore, Burlington, MA, USA). Approximately $4 \times 10^7$ HLE-B3 cells were lysed in RNA immunoprecipitation (RIP) lysis buffer and incubated with RIP buffer, including magnetic beads conjugated with 5 µg of anti-WTAP (41934; Cell Signaling Technology, Danvers, MA, USA) or rabbit IgG (Merck Millipore). Precipitated RNA was extracted and analyzed using quantitative PCR (qPCR). HOTAIR primers used for RIP are listed in Supplementary Table S2.

### Western Blotting

Proteins were extracted from mouse lens capsules and HLE-B3 cells using lysis buffer (Beyotime) containing 1% phenylmethylsulfonyl fluoride (ST506; Beyotime), and they were quantified using a BCA protein assay kit (P0010; Beyotime). Proteins were separated via SDS-PAGE, transferred onto polyvinylidene fluoride (PVDF) membranes (Merck Millipore), and analyzed by immunoblotting using antibodies (Supplementary Tables S3, S4). Bands were detected by an enhanced chemiluminescence (ECL) western blotting system (VILBER, Paris, France) and analyzed with ImageJ.

### Co-Immunoprecipitation

The effect of WTAP on METTL3 and METTL14 was analyzed using a Co-IP kit (Thermo Fisher Scientific). Briefly, $10^7$ cells were lysed in 600 µL of pre-cooled buffer and centrifuged (13,000*g* for 10 minutes); 10% of the lysate was used as input. The remaining cells were split and incubated overnight at 4°C with 5 µg WTAP (10200-1; Proteintech, Rosemont, IL, USA) or rabbit IgG (Cell Signaling Technology). The complexes were incubated with protein A/G beads for 2 hours at RT and washed three times. The proteins were then eluted with loading buffer, and purified proteins were tested using western blotting.

### Methylated RIP Sequencing and MeRIP-qPCR

Total RNA was extracted using TRIzol reagent. Methylated RIP (MeRIP) assays were performed according to the manufacturer's instructions (C11051-1; RiboBio). RNA (100 µg) from lncRNA HOTAIR overexpression and NC samples were fragmented into 100- to 150-bp fragments. One-tenth of the RNA was used as input, and the remainder was incubated with anti-m$^6$A (RiboBio) or IgG for 2 hours at 4°C. Methylated RNA was purified using a HiPure Serum/Plasma miRNA Kit (R4317-03; Magen, Guangzhou, China). The samples were sequenced by LC-Bio Technologies (Hangzhou, China). For MeRIP-qPCR, methylated RNA was reverse transcribed and analyzed using qPCR. The primers are listed in Supplementary Table S5, and PCR data were calculated using a previously reported method.[36]

### Wound Healing

Cells at 90% confluency in six-well plates were scraped with a sterile pipette tip (200 µL), washed twice with PBS, and incubated in a medium with 1% FBS at 37°C. Scratch widths were imaged at 0 and 48 hours and measured using ImageJ. The migration rate was calculated as the migration distance/original distance (0 hour).

### Transwell Assay

Cells ($3 \times 10^4$) were suspended in 200-µL serum-free medium and seeded in the upper chamber of a 24-well Transwell chamber with 8-µm pores filter (Falcon, 353097; Corning Inc., Corning, NY, USA). The lower chamber contained 600 µL of medium with treatments and 10% FBS. After 48 hours, the cells on top were removed, and the migrating cells were fixed in 4% PFA, stained with 1% crystal violet (C0121; Beyotime), and incubated at RT for 15 minutes. Migrating cells were counted in five fields under a microscope.

### Statistical Analysis

Data were analyzed using SPSS Statistics (IBM, Chicago, IL, USA) and Prism 8 (GraphPad, Boston, MA, USA). Results are expressed as mean ± standard error of at least three experiments. Student's *t*-test was used to compare two groups, and one-way analysis of variance (ANOVA) was used to analyze three or more groups. Statistical significance was set at $P < 0.05$.

## Results

### Upregulation of lncRNA HOTAIR in Mouse Cataract Surgery Model and TGF-β2–Treated Cells and Its Nuclear Localization

In vivo, vimentin mRNA levels increased at 3 and 5 days post-surgery; N-cadherin levels increased at 2, 3, and 5 days; and E-cadherin levels increased at 1 day but later decreased in the mouse cataract surgery model compared to the non-surgery (NS) group (Supplementary Figs. S1A–S1C). Further tests were performed 5 days after surgery (Fig. 1A). Detec-

Investigative Ophthalmology & Visual Science

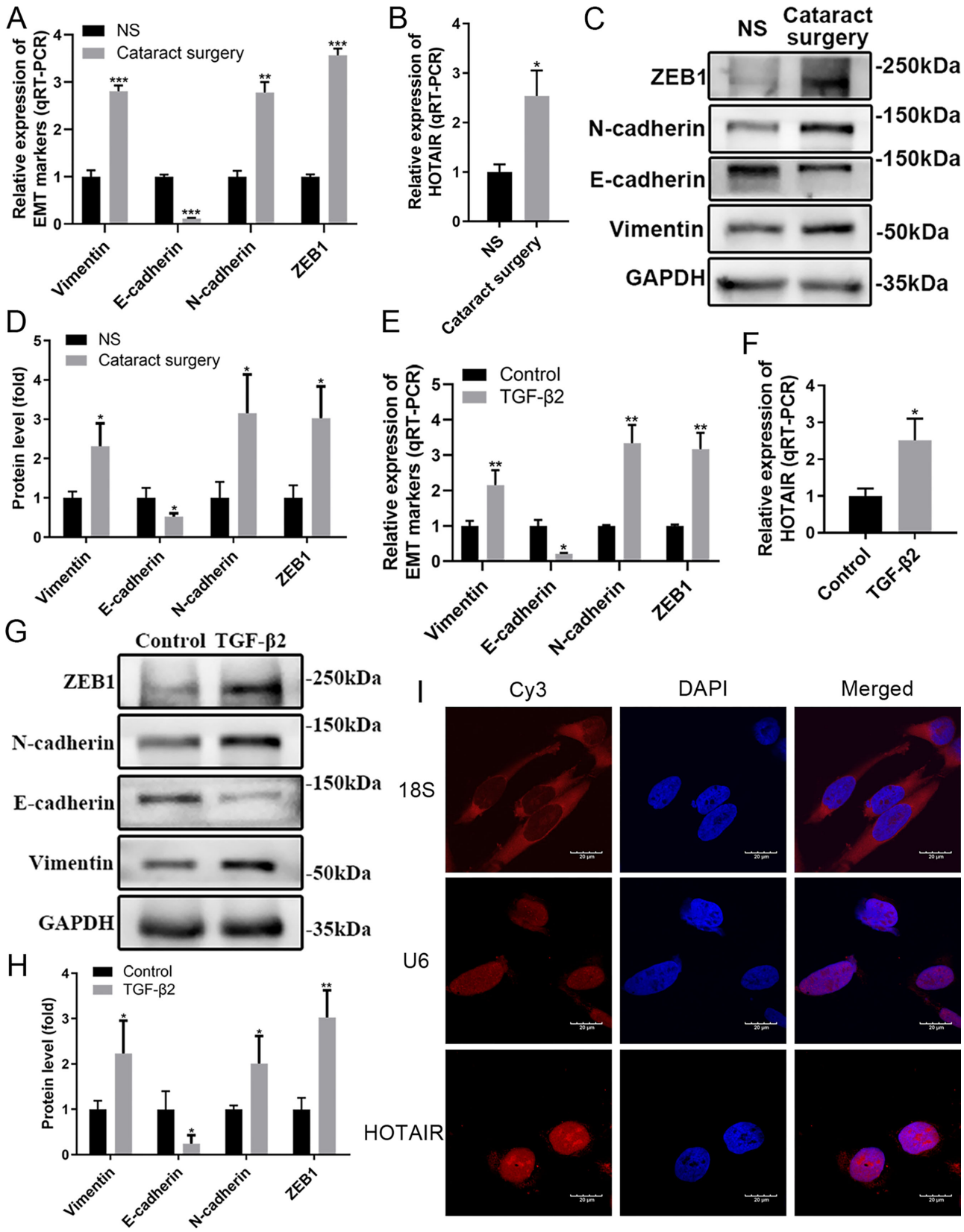


**Figure 1.** lncRNA HOTAIR expression and localization in the PCO model. (**A**, **B**) mRNA levels of lncRNA HOTAIR, vimentin, N-cadherin, E-cadherin, and ZEB1 in LECs of the NS group and 5 days post-surgery were determined using qRT-PCR analysis. (**C**, **D**) Protein levels of EMT markers in LECs of the NS group and 5 days post-surgery were determined using western blotting analysis. (**E**, **F**) lncRNA HOTAIR, vimentin, N-cadherin, E-cadherin, and ZEB1 mRNA levels after a 48-hour treatment of LECs with TGF-$\beta$2 (10 ng/mL). (**G**, **H**) Protein levels of EMT markers in TGF-$\beta$2 (10 ng/mL, 48 hours)–induced LECs. (**I**) Nuclear localization of lncRNA HOTAIR in HLE-B3 cells by RNA-FISH assay. *Scale bar*: 20 µm. Data are presented as mean ± SEM ($n$ = 3). Only $P < 0.05$ was considered significant. *$P < 0.05$, **$P < 0.01$, ***$P < 0.001$ (Student's $t$-test); ns, not significant.

Investigative Ophthalmology & Visual Science

tion of protein levels confirmed EMT in LECs after surgery (Figs. 1C, 1D).

In vitro, EMT of LECs induced by TGF-$\beta$2 is key for PCO.[8] HLE-B3 cells were treated with TGF-$\beta$2 at various concentrations for 0, 12, 24, 48, and 72 hours, and the mRNA/protein levels of HOTAIR, vimentin, E-cadherin, N-cadherin, and zinc finger E-box-binding homeobox (ZEB1) were measured using real-time quantitative reverse transcription PCR (qRT-PCR) (Supplementary Figs. S1E–S1H) and western blotting assays (Supplementary Figs. S1I–S1M). The ultimate model utilized 10 ng/mL TGF-$\beta$2 for 48 hours, demonstrating increased mRNA and protein levels of vimentin, ZEB1, and N-cadherin alongside decreased E-cadherin expression (Figs. 1E, 1G, 1H). HOTAIR levels significantly increased 5 days post-surgery in the mouse lens posterior capsules (Fig. 1B) and TGF-$\beta$2-treated cell lines (Fig. 1F). FISH confirmed the nuclear localization of HOTAIR in HLE-B3 cells (Fig. 1I). These findings reveal the high expression of HOTAIR in PCO models and its positive correlation with EMT markers, indicating a role in PCO development.

## HOTAIR Promotes TGF-$\beta$2–Induced Enhancement of Cell Viability, Proliferation, Migration, and EMT in LECs

The data shown above indicate a correlation between HOTAIR expression and PCO development. Cells in which HOTAIR expression was increased by lentivirus (Supplementary Figs. S2A, S2B) or inhibited by siRNA (Supplementary Figs. S2C, S2D) were constructed. Overexpression of HOTAIR promoted TGF-$\beta$2–induced reductions in E-cadherin and elevated vimentin and N-cadherin protein levels (Figs. 2A, 2B). CCK-8 and EdU assays showed that HOTAIR overexpression promoted cell viability and proliferation induced by TGF-$\beta$2 (Figs. 2C–2E). Transwell and wound healing assays revealed that migration induced by TGF-$\beta$2 was promoted by HOTAIR overexpression (Figs. 2F–2I).

In addition, western blotting analysis indicated that silencing HOTAIR reversed the reduction in E-cadherin and the elevation in vimentin and N-cadherin expression triggered by TGF-$\beta$2 (Figs. 3A, 3B). Cell viability (Fig. 3C), cell growth (Figs. 3D, 3E), and migration (Figs. 3F–3I) induced by TGF-$\beta$2 were suppressed by silencing HOTAIR. These findings support the involvement of HOTAIR in regulating the EMT of LECs.

## m$^6$A Methylation Level Was Positively Correlated With EMT of LECs In Vitro and In Vivo; WTAP, METTL3, and METTL14 Were Located in the Nucleus of LECs

No sex-related differences were observed in the expression levels of lncRNA HOTAIR and m$^6$A methylases in 10-week-old mice (Supplementary Fig. S3). In contrast to the control group, total m$^6$A levels increased in LECs of mouse capsules at 2 to 5 days post-surgery (Fig. 4A) and in TGF-$\beta$2–treated HLE-B3 cells (Fig. 4B), consistent with the EMT marker trends (Fig. 1). WTAP and METTL3 mRNA and protein levels were significantly upregulated, whereas METTL14 was downregulated in the cataract surgery model (Figs. 4C–4E) and TGF-$\beta$2–treated cells (Figs. 4F–4H), which was confirmed by immunofluorescence analysis of the cataract surgery model (Figs. 4J–4L). IF analysis revealed the nuclear localization of WTAP, METTL3, and METTL14 in HLE-B3 cells (Fig. 4I). These findings suggest that m$^6$A methylation levels correlate with EMT, highlighting its role in PCO development.

## Interactions Between lncRNA HOTAIR and WTAP Protein in LECs

Interactions between lncRNAs and RNA-binding proteins (RBPs),[37] traditionally seen as RNA controllers, show that RNA modulates RBP functions.[38] Because HOTAIR is nuclear (Fig. 1I) and ncRNA can bind to WTAP,[28] we examined the HOTAIR/WTAP complex in LECs. CatRAPID[39] predicted direct interactions between HOTAIR and WTAP (Supplementary Fig. S4A) and validated them via RIP–qRT-PCR (Figs. 5A, 5B). Dual RNA FISH and IF confirmed that HOTAIR colocalized with WTAP in LEC nuclei (Supplementary Fig. S4B), indicating an interaction.

## HOTAIR Promotes Assembly of the WTAP/METTL3/METTL14 Complex to Enhance Total m$^6$A Levels in TGF-$\beta$2–Induced Cells

WTAP overexpression and low-expression HLE-B3 cells were constructed (Supplementary Fig. S5). qRT-PCR showed no difference in HOTAIR levels between WTAP overexpression or knockdown cells (Figs. 5C, 5D). Western blotting and IF revealed that altering HOTAIR did not affect WTAP, METTL3, or METTL14 protein levels or WTAP localization (Figs. 5F, 5G, 5I–5K). However, HOTAIR overexpression promoted the decrease in METTL14 and increase in WTAP and METTL3 protein expression, as well as an elevation in total m$^6$A levels induced by TGF-$\beta$2 in LECs (Figs. 5E–5G), with knockdown of HOTAIR showing opposite trends (Figs. 5H–5J). Co-immunoprecipitation experiments confirmed that HOTAIR knockdown reduced the mutual effect between endogenous WTAP and METTL3 and METTL14 (Fig. 5L; Supplementary Figs. S4C, S4D).

## WTAP Knockdown Reverses the Enhanced EMT, Cell Proliferation, and Migration Induced by HOTAIR Overexpression

Western blotting analysis showed that WTAP knockdown reversed the decline in E-cadherin and the increase in N-cadherin and vimentin protein levels caused by HOTAIR overexpression in TGF-$\beta$2–induced cells (Figs. 6A–6D). Furthermore, CCK-8, EdU, Transwell, and wound healing assays demonstrated that WTAP knockdown reversed the HOTAIR overexpression-induced increases in cell proliferation (Figs. 6E, 6F), viability (Fig. 6G), and migration (Figs. 6H–6K) in TGF-$\beta$2–treated cells. These results indicate that enhancement of EMT, cell proliferation, and migration of LECs was promoted by HOTAIR via WTAP-mediated m$^6$A methylation.

## MeRIP-Seq Analysis of m$^6$A Modifications in lncRNA HOTAIR-Overexpressing Cells

RNA-seq revealed that 54 genes ($\log_2$FC $\leq -1$; $P < 0.05$) were downregulated and 92 ($\log_2$FC $\geq 1$; $P < 0.05$) were upregulated in HOTAIR-overexpressing HLE-B3 cells

Investigative Ophthalmology & Visual Science

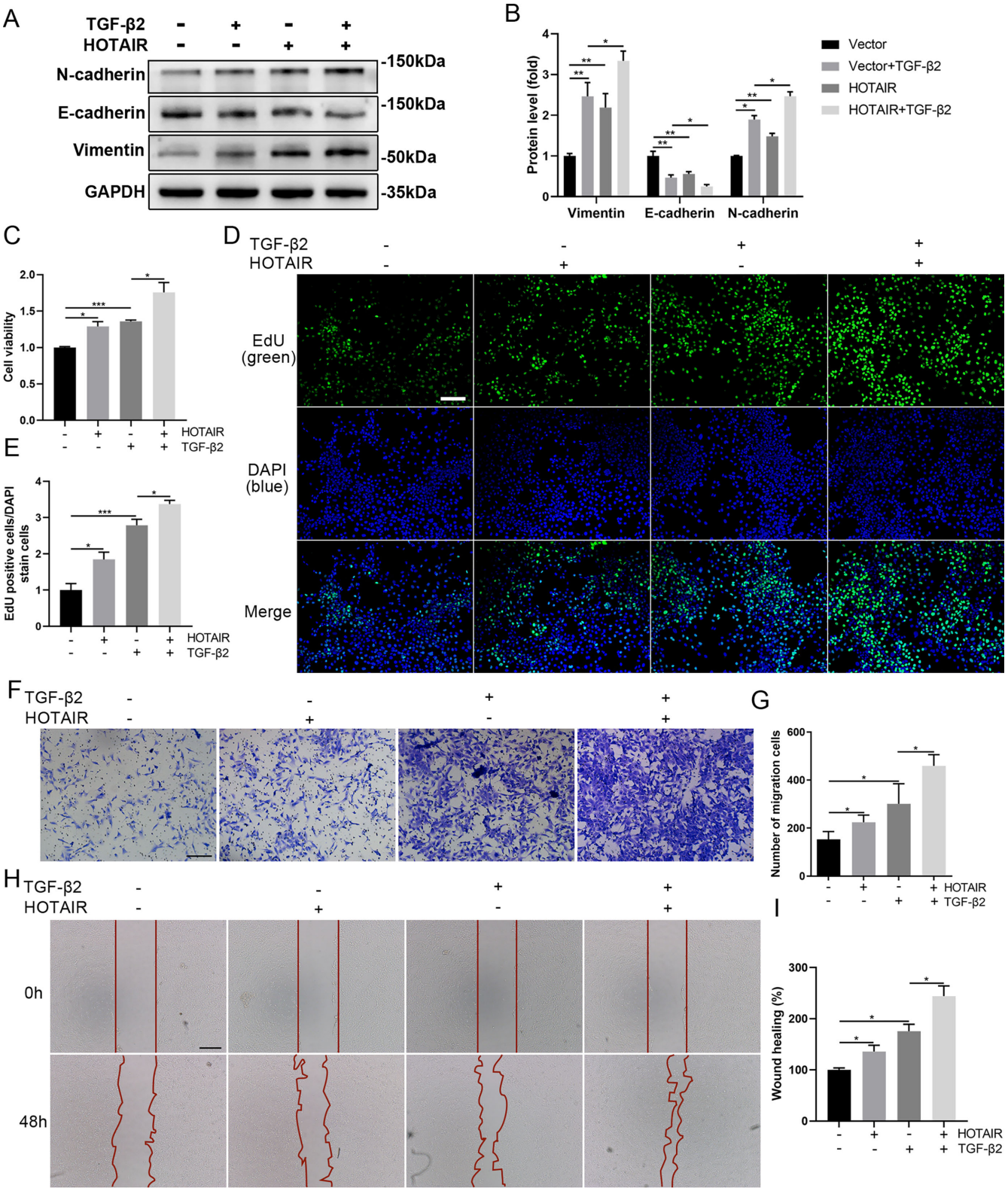


**Figure 2.** LncRNA HOTAIR overexpression promotes EMT, cell viability, proliferation, and migration of TGF-l –treated LECs. (**A**, **B**) After transfection of the HLE-B3 cells with HOTAIR overexpression or NC lentivirus followed by treatment with 10 ng/mL TGF-$\beta$2 for 48 hours, western blotting indicated vimentin, N-cadherin, and E-cadherin protein levels. (**C**) The viability of HLE-B3 cells was examined using the CCK-8 assay. (**D**, **E**) The proliferation of HLE-B3 cells was examined using EdU analysis. *Scale bar*: 200 µm. (**F**, **G**) Transwell migration results expressed as the number of migrated cells. *Scale bar*: 200 µm. (**H**, **I**) Wound healing assay showed cell migration at 0 and 48 hours. *Scale bar*: 100 µm. Data are presented as mean ± SEM ($n$ = 3). Only $P < 0.05$ was considered significant. *$P < 0.05$, **$P < 0.01$, ***$P < 0.001$ (one-way ANOVA); ns, not significant.

Investigative Ophthalmology & Visual Science

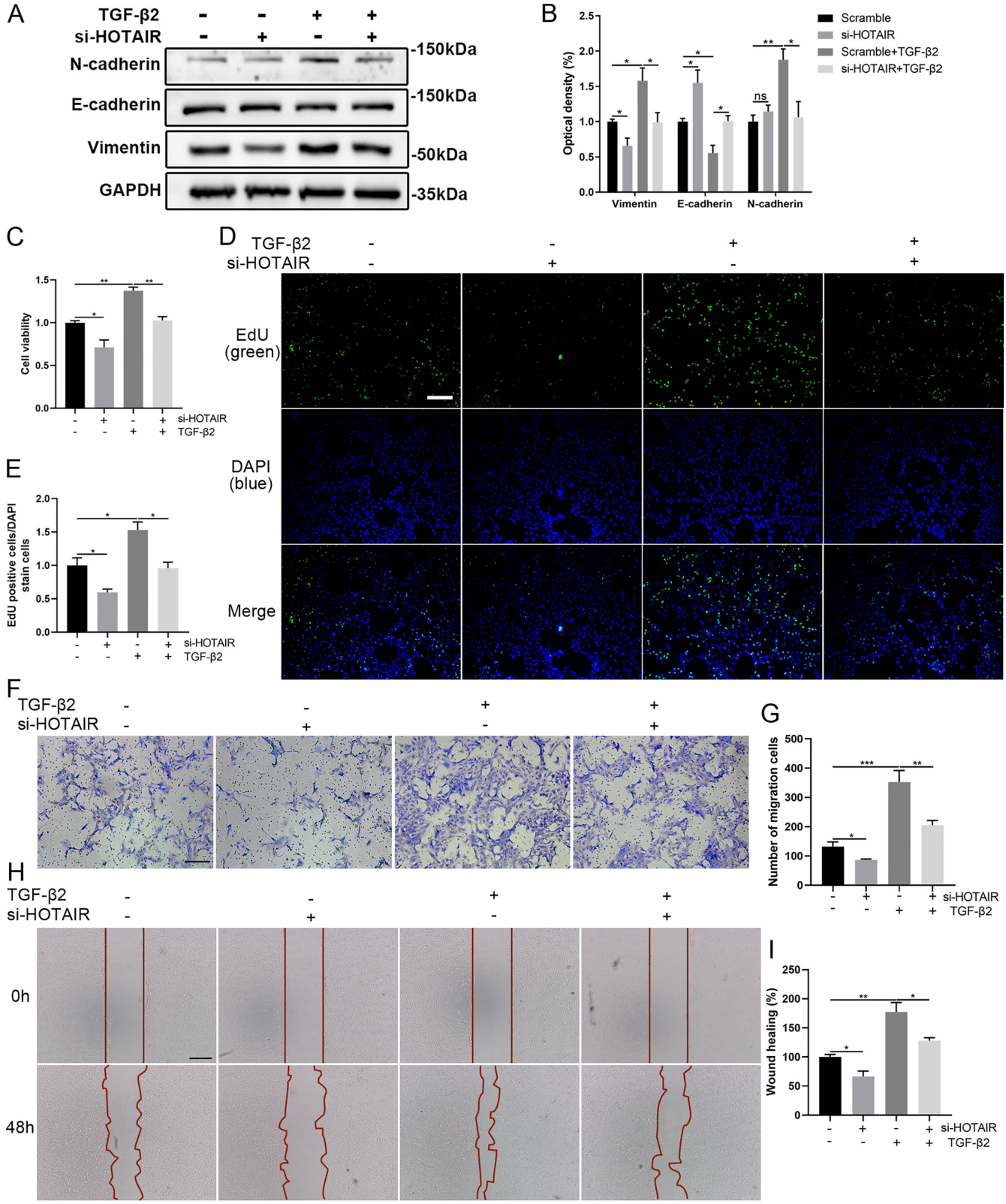


**Figure 3.** LncRNA HOTAIR knockdown inhibits TGF-bi–induced EMT, cell viability, proliferation, and migration of LECs. (**A**, **B**) After transfection of the HLE-B3 cells with si-HOTAIR or si-NC followed by treatment with 10 ng/mL TGF-$\beta$2 for 48 hours, western blotting indicated EMT marker protein levels. (**C**) The viability of HLE-B3 cells was examined using the CCK-8 assay. (**D**, **E**) The proliferation of HLE-B3 cells was examined using EdU analysis. *Scale bar*: 200 µm. (**F**, **G**) Transwell migration results expressed as the number of migrated cells. *Scale bar*: 200 µm. (**H**, **I**) Wound healing assay showed cell migration at 0 and 48 hours. *Scale bar*: 100 µm. Data are presented as mean ± SEM ($n = 3$). Only $P < 0.05$ was considered significant. *$P < 0.05$, **$P < 0.01$, ***$P < 0.001$ (one-way ANOVA); ns, not significant.

Investigative Ophthalmology & Visual Science

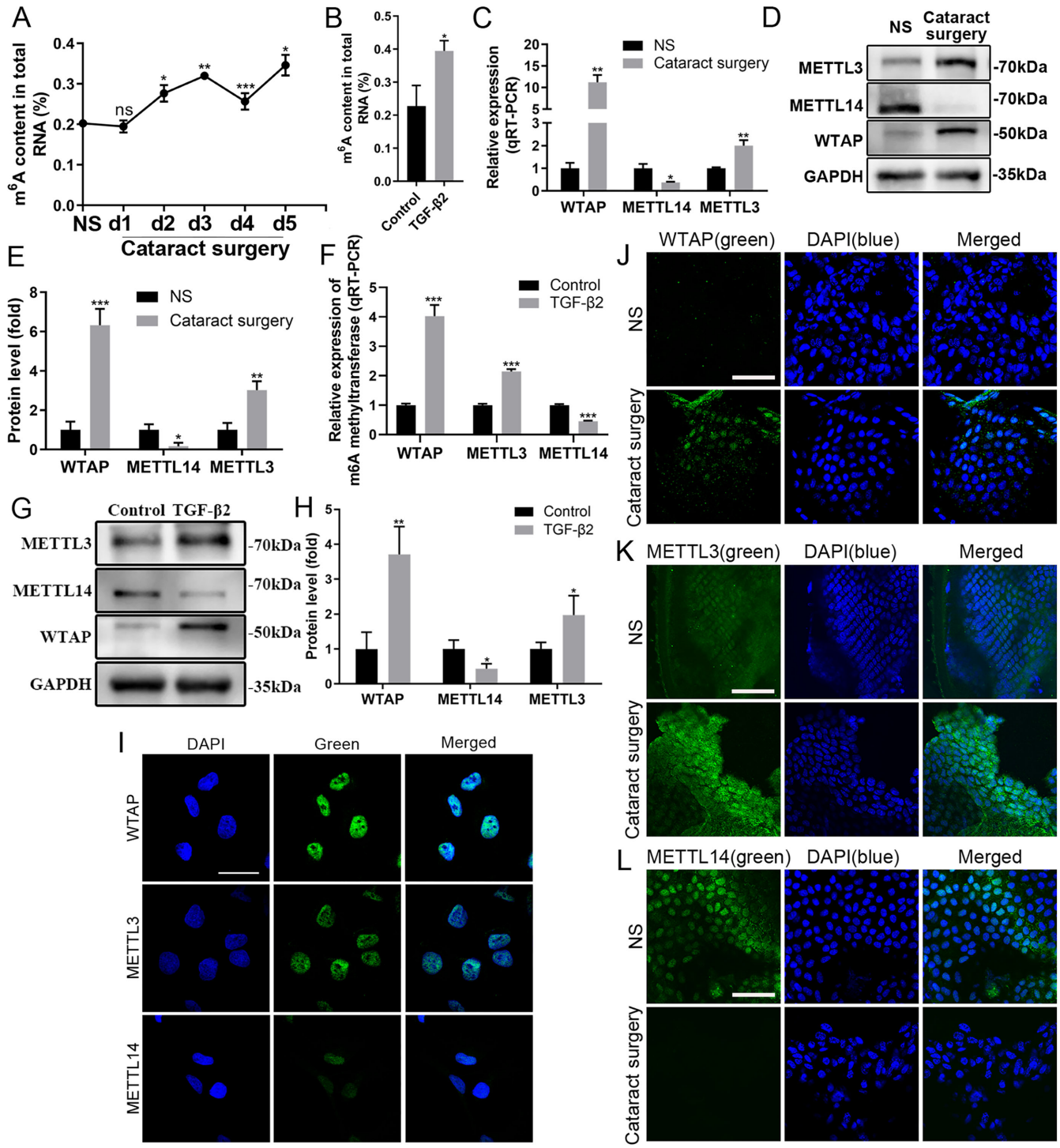


**Figure 4.** Total m$^6$A levels and expression and localization of WTAP, METTL3, and METTL14 in the PCO model. (**A**) RNA m$^6$A quantification assay showed total m$^6$A modification levels in LECs from the NS and 1, 2, 3, 4, and 5 days after cataract surgery. (**B**) Total m$^6$A modification level in TGF-$\beta$2 (10 ng/mL)–treated LECs after 48 hours. (**C–E**) mRNA and protein levels of WTAP, METTL3, and METTL14 in LECs from the NS group and 5 days post-surgery determined using qRT-PCR and western blotting analysis. (**F–H**) mRNA and protein levels of WTAP, METTL3, and METTL14 in TGF-$\beta$2 (10 ng/mL)–treated LECs after 48 hours. (**I**) IF staining assay indicated nuclear localization of WTAP, METTL3, and METTL14 (*green*) in HLE-B3 cells, with nuclei stained with DAPI (*blue*). *Scale bar*: 40 µm. (**J–L**) IF staining assay indicated the expression levels of WTAP, METTL3, and METTL14 (*green*) in lens capsules of the NS group and 5 days post-surgery, with nuclei stained with DAPI (*blue*). *Scale bar*: 50 µm. Data are presented as mean ± SEM ($n = 3$). Only $P < 0.05$ was considered significant. *$P < 0.05$, **$P < 0.01$, ***$P < 0.001$ (Student's *t*-test); ns, not significant.

Investigative Ophthalmology & Visual Science

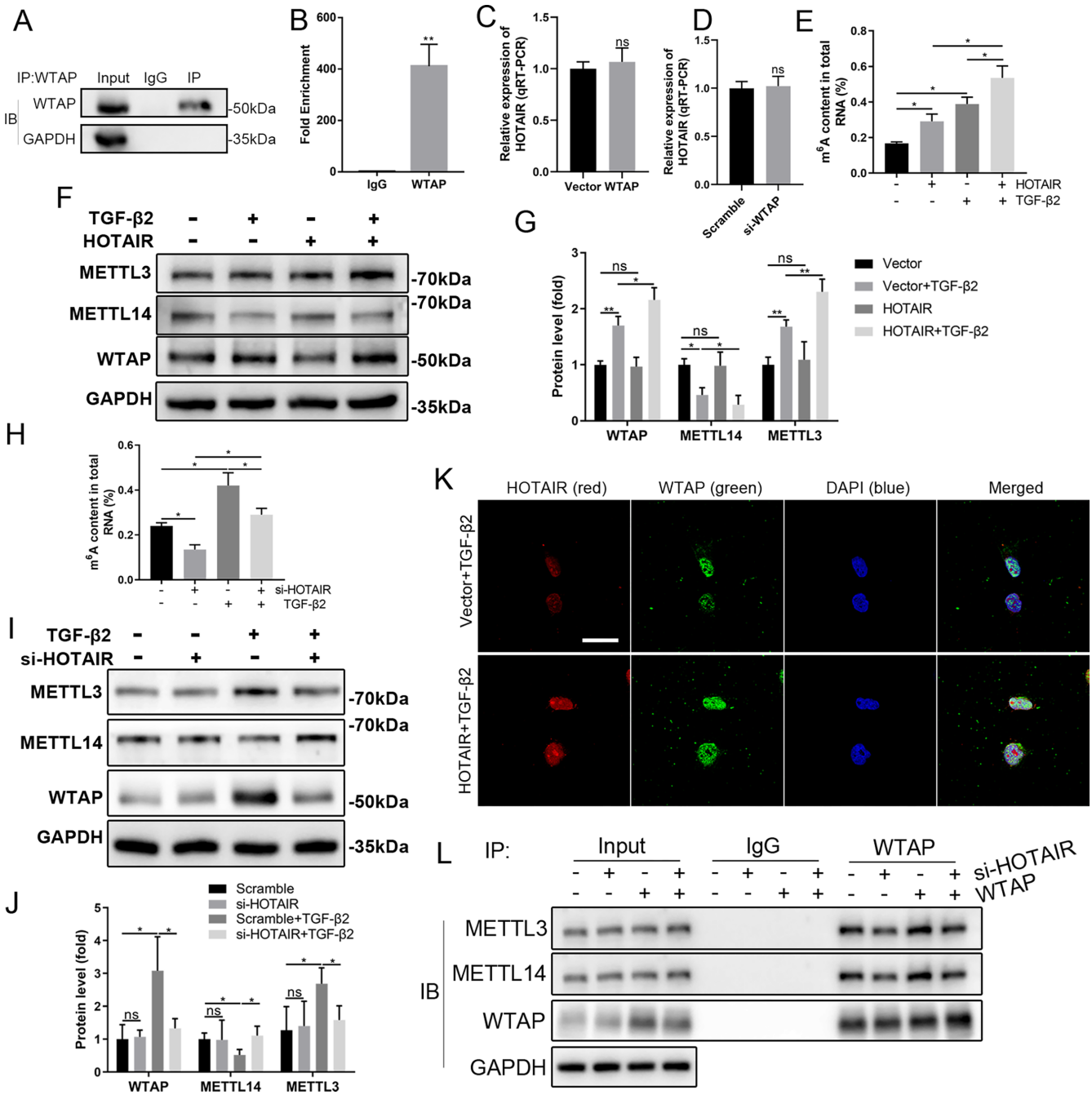


**Figure 5.** Interaction between lncRNA HOTAIR and WTAP protein and the effect of HOTAIR on the WTAP/METTL3/METTL14 complex and total m$^6$A level in EMT of LECs. (**A**, **B**) RIP and qRT-PCR showed the interaction between HOTAIR and WTAP. (**C**, **D**) HOTAIR expression levels were examined using qRT-PCR in HLE-B3 cells with overexpression and knockdown of WTAP. (**E**, **H**) Total m$^6$A level in HOTAIR overexpression and knockdown LECs after TGF-$\beta$2 treatment (10 ng/mL for 48 hours). (**F**, **G**, **I**, **J**) Western blotting indicated WTAP, METTL3, and METTL14 protein levels in HOTAIR overexpression and knockdown LECs after TGF-$\beta$2 treatment (10 ng/mL for 48 hours). (**K**) Dual RNA-FISH and IF indicated the colocalization of HOTAIR and WTAP in TGF-$\beta$2–induced HLE-B3 cells with low or overexpression of HOTAIR. *Scale bar*: 30 µm. (**L**) Co-IP and western blotting results showed the binding efficiency of WTAP with METTL3 and METTL14 in LECs transfected with si-NC or si- HOTAIR, and co-transfected with NC or WTAP overexpression lentivirus. Data are presented as mean ± SEM ($n = 3$). Only $P < 0.05$ was considered significant. *$P < 0.05$, **$P < 0.01$, ***$P < 0.001$ (Student's *t*-test and one-way ANOVA); ns, not significant.

(Fig. 7A). Heat maps showed a strong consistency between the groups (Fig. 7B), and GGAC motifs were enriched at m$^6$A sites (Fig. 7C). The m$^6$A-seq identified 33,971 and 32,660 peaks in NC and HOTAIR overexpression cells, respectively ($P < 0.05$), with 18,916 shared peaks (Fig. 7D). Peaks were enriched in the 3′UTR (Figs. 7E, 7F). Most m$^6$A-marked transcript types were protein coding (Supplementary Fig. S6C). Gene Ontology (GO) analysis linked differential peaks to protein binding (Fig. 7G), and Kyoto Encyclopedia of Genes and Genomes (KEGG) showed associations with ECM–receptor interaction and TNF signaling pathways (Fig. 7H).

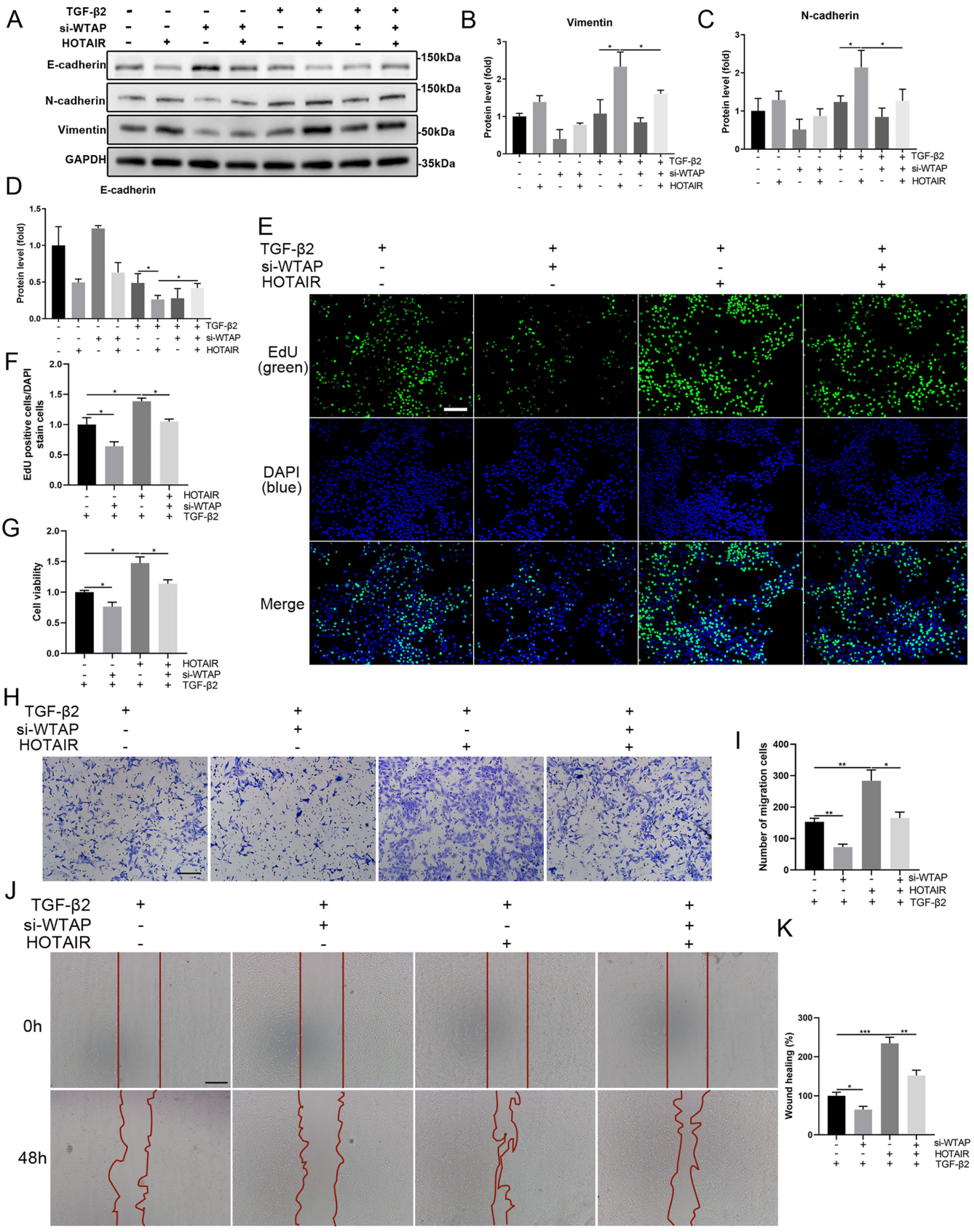


**Figure 6.** Knockdown of WTAP inhibits the enhanced EMT, cell proliferation and migration of LECs induced by overexpression of lncRNA HOTAIR. (**A–D**) Western blotting results showed vimentin, N-cadherin, and E-cadherin protein levels in LECs with NC or HOTAIR overexpression lentivirus and co-transfected with si-NC or si-WTAP. (**E**, **F**) Cell proliferation was tested using EdU assay. (**G**) Cell viability was detected using CCK-8 assay. (**H**, **I**) Transwell migration assay showed the number of migrated cells. *Scale bar*: 200 µm. (**J**, **K**) Wound healing assay showed migrating cells. *Scale bar*: 100 µm. Data are presented as mean ± SEM ($n = 3$). Only $P < 0.05$ was considered significant. $^*P < 0.05$, $^{**}P < 0.01$, $^{***}P < 0.001$ (one-way ANOVA).

Investigative Ophthalmology & Visual Science

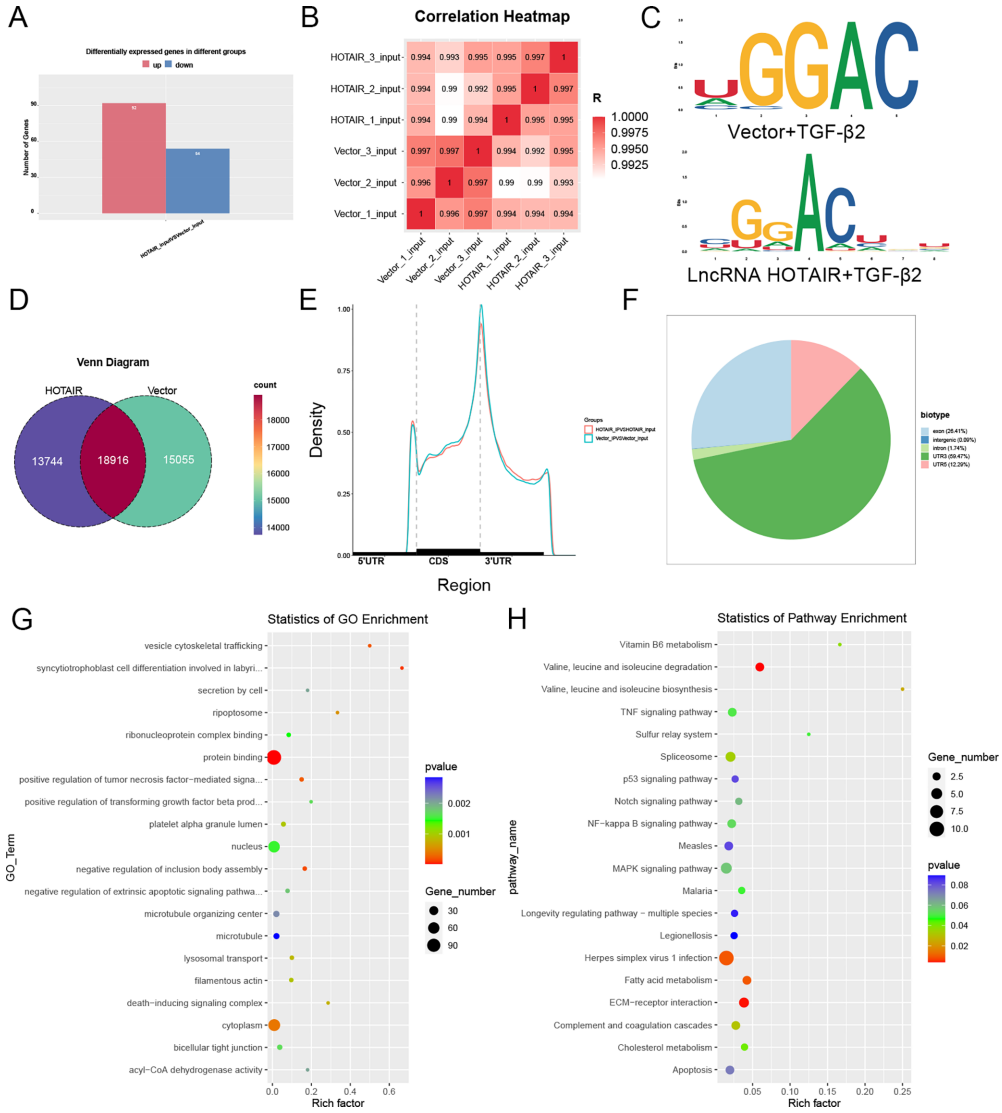


**Figure 7.** Identification of the lncRNA HOTAIR/WTAP complex targets via RNA-seq and MeRIP-seq. (**A**) DEGs identified by RNA-seq in NC and HOTAIR overexpression HLE-B3 cells with TGF-$\beta$2 treatment. (**B**) Heatmap showed consistency between NC and HOTAIR overexpression groups. (**C**) Predominant consensus motif GGAC. (**D**) The number of m$^6$A peaks in NC and HOTAIR overexpression groups. (**E**) Density distribution of m$^6$A peaks across mRNA transcripts. (**F**) Distribution of different m$^6$A peaks in NC and HOTAIR overexpression groups. (**G**, **H**) GO and KEGG enrichment analysis of the genes of differential peaks.

## Regulation of THBS1 by the HOTAIR/WTAP Complex in EMT

MeRIP-seq confirmed that lncRNA HOTAIR regulates m$^6$A modification in HLE-B3 cells. Five EMT-promoting genes with elevated m$^6$A levels were tested: *FOSB*, *KLF6*, *THBS1*, *FZD5*, and *LZTS1*. For MeRIP-qPCR analysis, according to the predicted m$^6$A motif sites, PCR primers were designed for each gene. This showed that HOTAIR m$^6$A level remained unchanged after TGF-$\beta$2 treatment (Fig. 8A). The m$^6$A modification levels of *LZTS1*, *FZD5*, and *THBS1* mRNA were enhanced by HOTAIR overexpression. In contrast, the m$^6$A modification levels of other genes did not change. Among these, only THBS1 exhibited changes in m$^6$A modification levels at all potential motif sites (Figs. 8B–8F). In TGF-$\beta$2–treated LECs, only the mRNA expression of *THBS1* was enhanced by HOTAIR overexpression, whereas the mRNA levels of other genes were not affected by HOTAIR (Fig. 8G).

After TGF-$\beta$2 treatment and HOTAIR overexpression, THBS1 protein expression was enhanced, whereas the expression of the other genes remained unchanged (Figs. 9A–9F). Western blotting revealed increased expression of THBS1 in TGF-$\beta$2–treated cells overexpressing WTAP (Figs. 9G, 9H). MeRIP-qPCR showed that WTAP overexpression reversed the THBS1 m$^6$A reduction caused by HOTAIR knockdown (Figs. 9I–9K). These findings indicate a positive correlation between HOTAIR/WTAP and THBS1 in the EMT regulation of LECs.

## HOTAIR/WTAP Complex Promotes EMT by Regulating THBS1 Expression

In vivo and in vitro, THBS1 was significantly increased in TGF-$\beta$2–induced HLE-B3 and mouse cataract surgery models of PCO, as determined using qRT-PCR (Figs. 10A, 10D),

Investigative Ophthalmology & Visual Science

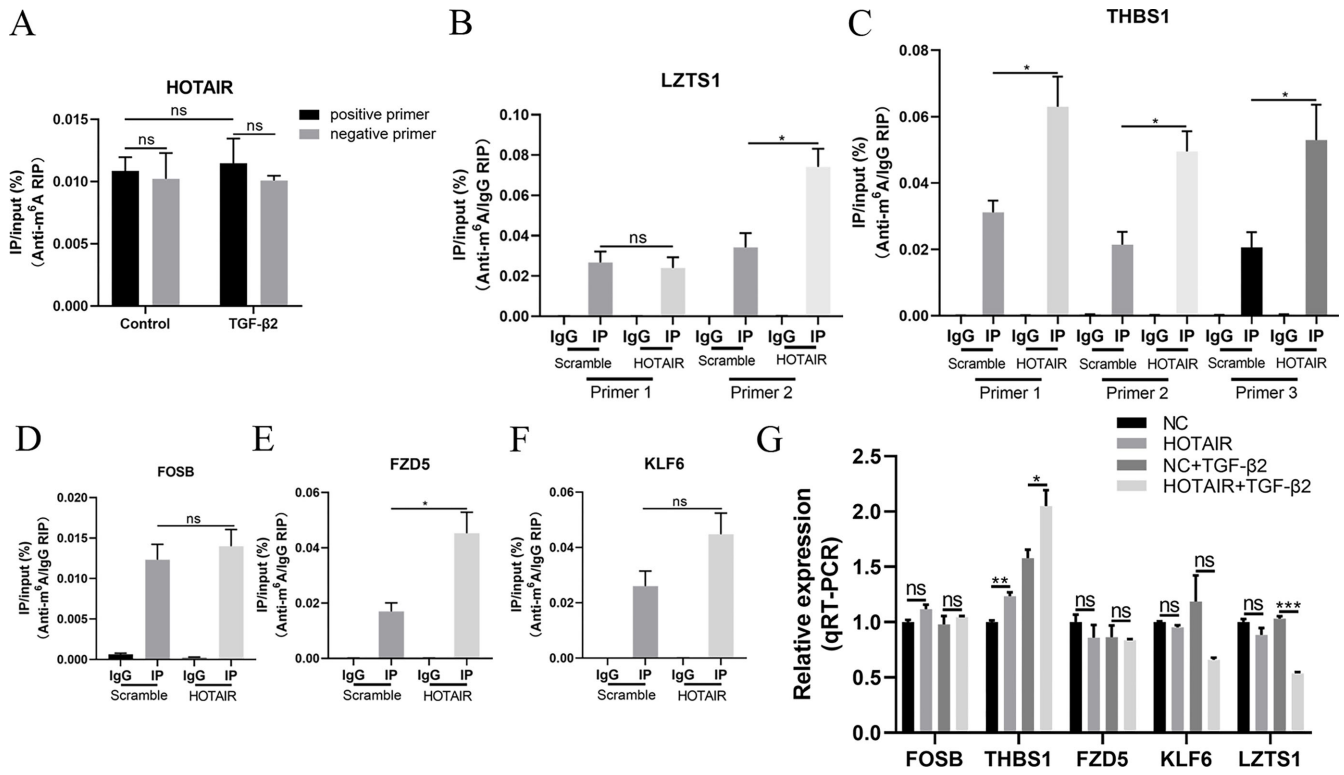


**Figure 8.** THBS1 serves as the downstream marker of the HOTAIR/WTAP complex in LECs EMT. (**A**) m$^6$A levels of lncRNA HOTAIR did not change in the control group or TGF-$\beta$2 treatment group. (**B–F**) RIP-qPCR revealed the relative m$^6$A modification levels of five mRNA candidates (*LZTS1*, *THBS1*, *FOSB*, *KLF6*, and *FZD5*) in TGF-$\beta$2–induced HLE-B3 cells stably transfected with NC or HOTAIR overexpression lentivirus. (**G**) The levels of five mRNA candidates in TGF-$\beta$2–induced HLE-B3 cells stably transfected with NC or HOTAIR overexpression lentivirus were detected using qRT-PCR assay. Data are presented as mean ± SEM ($n$ = 3). Only $P < 0.05$ was considered significant. *$P < 0.05$, **$P < 0.01$, ***$P < 0.001$ (Student's $t$-test and one-way ANOVA); ns, not significant.

western blotting (Figs. 10B, 10C, 10E, 10F), and IF assays (Figs. 10G, 10H). In TGF-$\beta$2–induced cells, THBS1 knockdown restored the HOTAIR overexpression-induced reduction in E-cadherin and increment in vimentin and N-cadherin protein levels (Figs. 11A–11D; Supplementary Fig. S7). IF staining confirmed the changes in vimentin expression (Fig. 11E). THBS1 knockdown also inhibited the enhanced wound healing and migration abilities of HOTAIR-overexpressing cells (Figs. 11F–11I). These findings confirm that the HOTAIR/WTAP complex influences EMT in LECs by regulating THBS1 expression.

## Discussion

m$^6$A mRNA modifications contribute to several diseases; however, eye diseases differ because of their unique physiology and immune privilege. Therefore, understanding m$^6$A methylation in eye diseases is essential. This study shows that lncRNA HOTAIR interacts with WTAP, a key m$^6$A writer, promoting EMT in LECs by upregulating m$^6$A modification and THBS1 expression levels. These discoveries point to the significance of m$^6$A in PCO pathogenesis and a novel interaction between HOTAIR and WTAP.

Research on aberrant m$^6$A modification in eye diseases, including cataracts and diabetic retinopathy, is in its infancy.[40] Abnormal expression of m$^6$A writers, erasers, and readers is connected with LEC apoptosis in cataracts,[41–44] suggesting that m$^6$A may regulate LEC function. The m$^6$A modification of mRNA can regulate EMT in tumor cells; however, its role in LECs remains unclear. This study revealed increased m$^6$A levels in mouse LECs after cataract surgery and TGF-$\beta$2–induced human LECs. METTL3 and WTAP levels were elevated, whereas METTL14 level was decreased, differing from tumor cells due to cell and pathogen variations. m$^6$A modifications and related enzymes were significantly altered during EMT in LECs, suggesting their role in PCO progression.

The cell viability, proliferation, migration, EMT markers, and total m$^6$A levels induced by TGF-$\beta$2 were significantly influenced by increased lncRNA HOTAIR expression in PCO models. In contrast to a previous study,[27] we identified nuclear-localized HOTAIR in LECs, suggesting its potential to interact with genes or RBPs. HOTAIR, which is not modified by m$^6$A,[45,46] promotes WTAP binding to METTL3 and METTL14, regulating m$^6$A modification without affecting their expression. Furthermore, the N-terminal nuclear localization signal of WTAP[47] suggests that HOTAIR binding may alter the spatial conformation of the METTL3/14 complex. ncRNAs have been shown to target WTAP[30,48] or modulate IGF2BP2 ubiquitination and stability,[49,50] thus regulating m$^6$A enzymes via diverse mechanisms. LncRNAs may regulate fibrosis, migration, and EMT in LECs by acting as competing endogenous RNAs, sponging microRNAs[20–22] and influencing RBP function.[38] Our study suggests a new mechanism wherein HOTAIR binds to nuclear WTAP to regulate

Investigative Ophthalmology & Visual Science

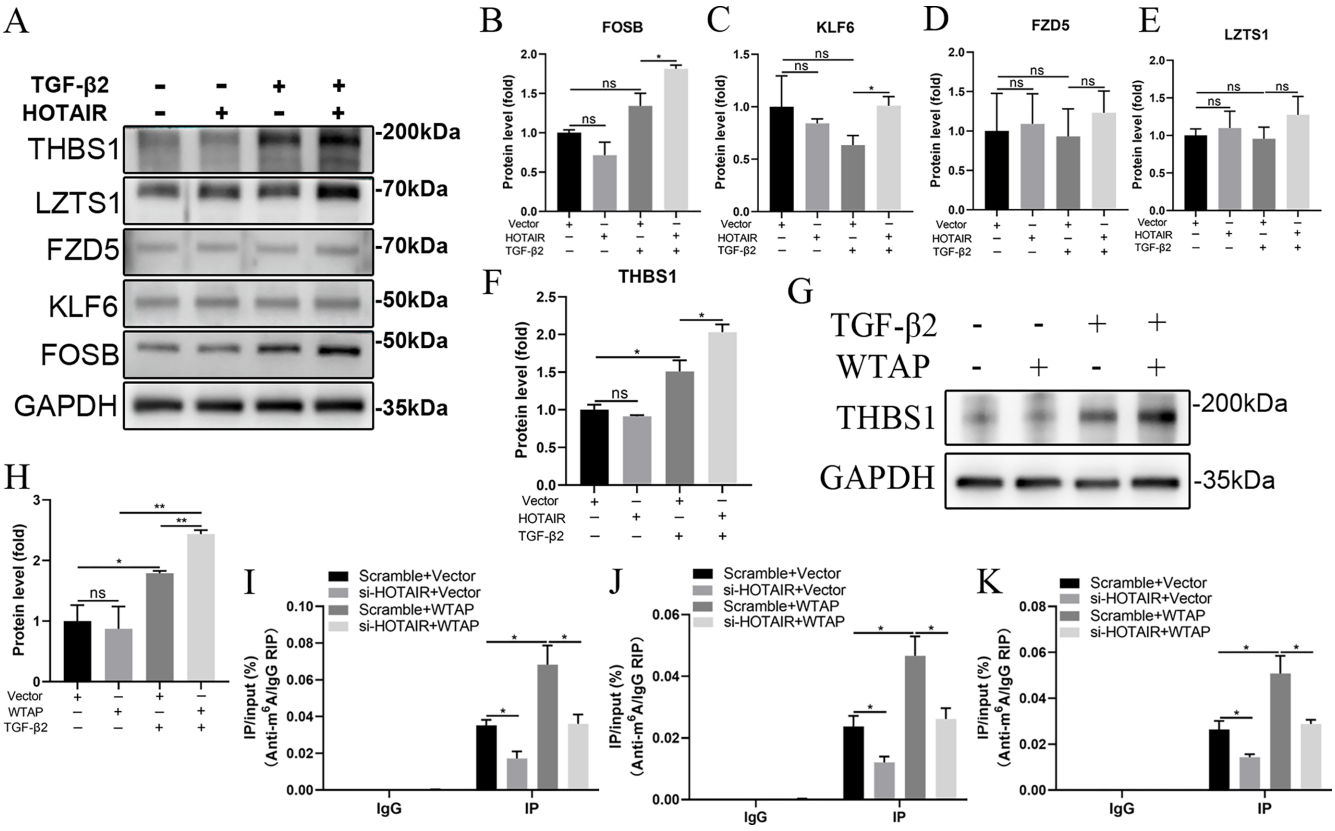


**Figure 9.** HOTAIR/WTAP complex enhances the expression of THBS1 in an m$^6$A-dependent manner in the EMT of LECs. (**A**–**F**) Western blotting showed the expression levels of *LZTS1*, *THBS1*, *FOSB*, *KLF6*, and *FZD5* in TGF-$\beta$2–induced HLE-B3 with stable NC or HOTAIR overexpression lentivirus transfection. (**G**, **H**) Western blotting showed THBS1 protein levels in TGF-$\beta$2–induced WTAP overexpression HLE-B3 cells. (**I**–**K**) After TGF-$\beta$2–induced HLE-B3 cells were transfected with si-NC or si-HOTAIR and then co-transfected with NC or WTAP overexpression lentivirus, RIP-qPCR showed the relative m$^6$A modification levels of *THBS1* mRNA. Data are presented as mean ± SEM ($n = 3$). Only $P < 0.05$ was considered significant. *$P < 0.05$, **$P < 0.01$, ***$P < 0.001$ (one-way ANOVA); ns, not significant.

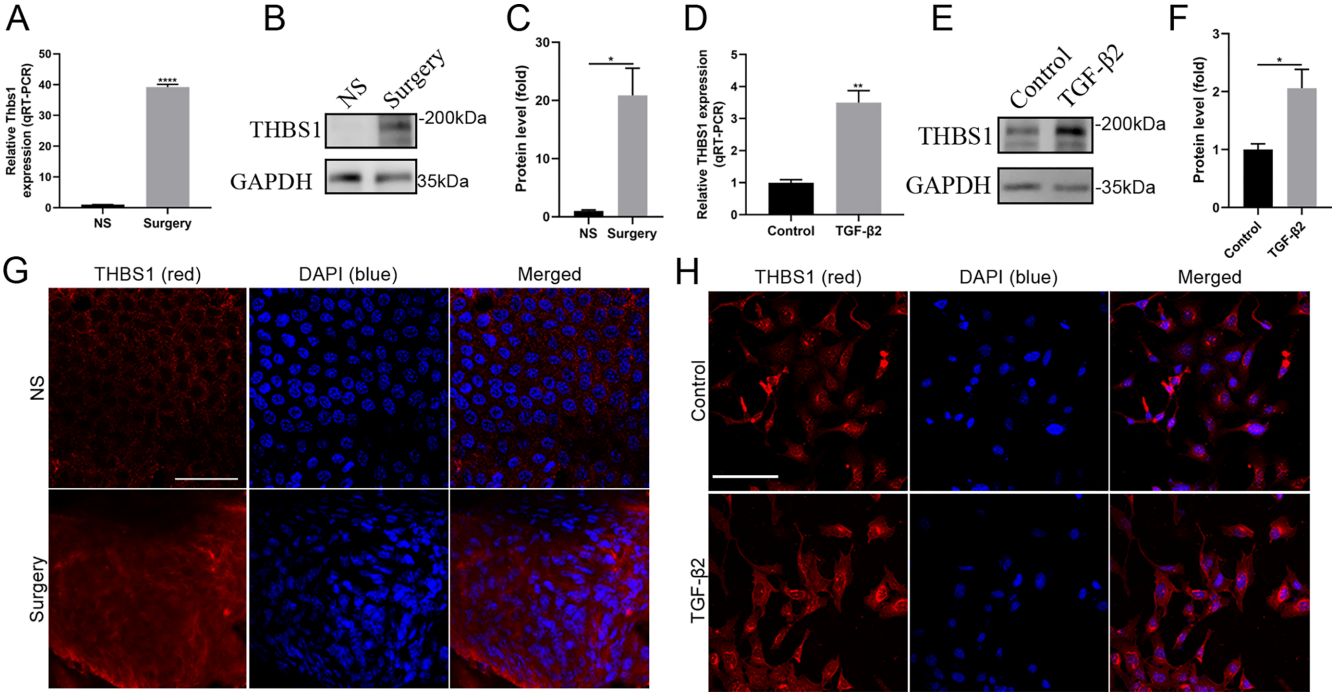


**Figure 10.** The expression of THBS1 in TGF-$\beta$2–induced cells and mouse cataract surgery models of PCO. (**A**–**C**, **G**) The expression levels of THBS1 in LECs from the NS group and 5 days post-surgery were determined using qRT-PCR, western blotting, and immunofluorescence staining. *Scale bar*: 50 µm. (**D**–**F**, **H**) The expression levels of THBS1 in LECs after TGF-$\beta$2 (10 ng/mL) treatment for 48 hours. *Scale bar*: 100 µm. Data are presented as mean ± SEM ($n = 3$). Only $P < 0.05$ was considered significant. *$P < 0.05$, **$P < 0.01$, ***$P < 0.001$, ****$P < 0.0001$ (Student's *t*-test); ns, not significant.

Investigative Ophthalmology & Visual Science

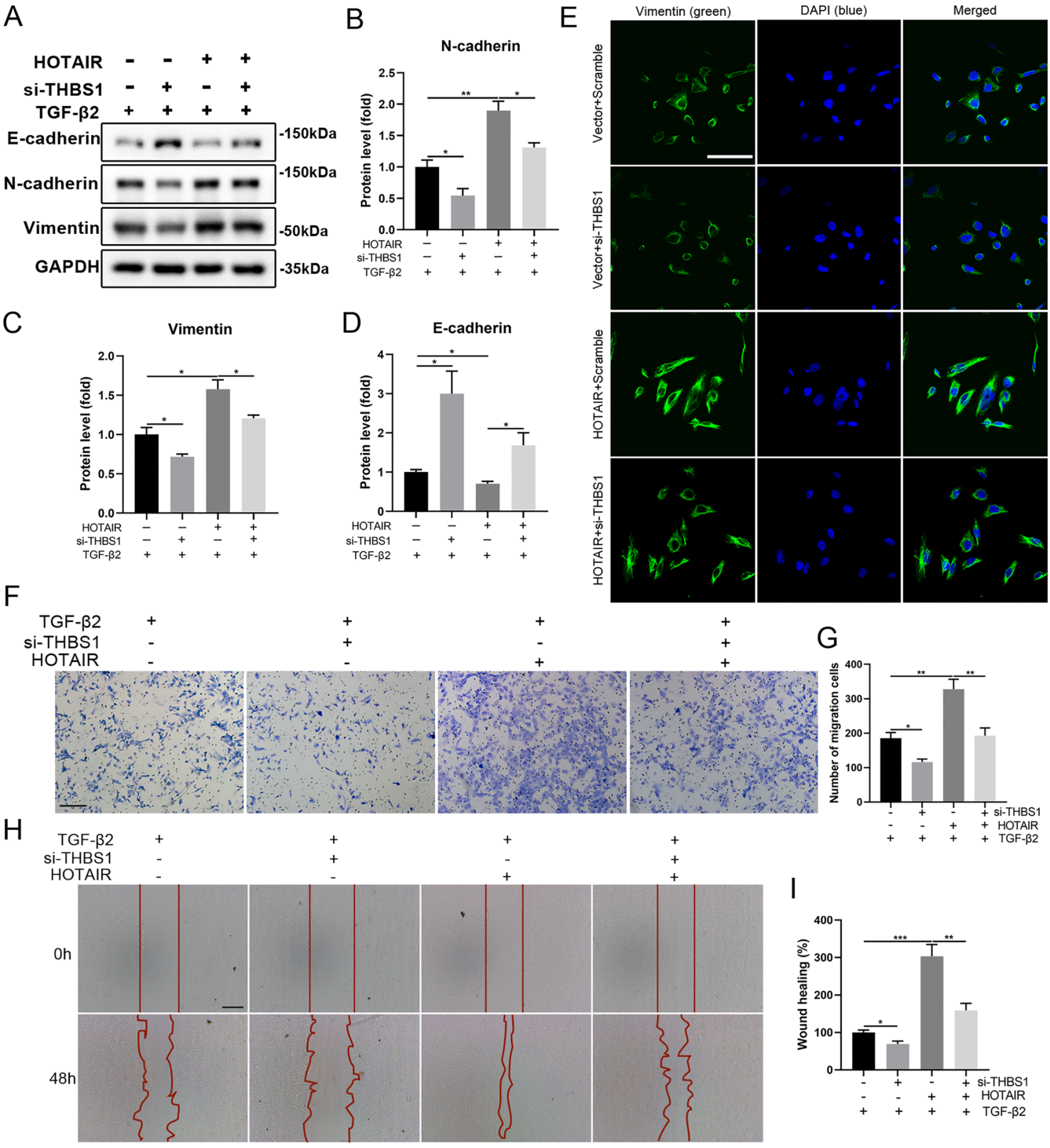


**Figure 11.** HOTAIR/WTAP complex promotes EMT of LECs by enhancing THBS1 expression. (**A–D**) Western blotting analysis showed the expression levels of EMT markers after TGF-$\beta$2–induced HLE-B3 cells were transfected with NC or HOTAIR overexpression followed by co-transfection with si-NC or si-THBS1. (**E**) IF staining showed the vimentin level. *Scale bar*: 100 µm. (**F**, **G**) Transwell assay showed migrating cells in TGF-$\beta$2-induced HOTAIR overexpression HLE-B3 cells with THBS1 low expression. *Scale bar*: 200 µm. (**H**, **I**) Wound healing assay showed migrating cells in TGF-$\beta$2–induced HOTAIR overexpression HLE-B3 cells with THBS1 low expression. *Scale bar*: 100 µm. Data are presented as mean ± SEM ($n = 3$). Only $P < 0.05$ was considered significant. *$P < 0.05$, **$P < 0.01$, ***$P < 0.001$, ****$P < 0.0001$ (one-way ANOVA); ns, not significant.

EMT in LECs. However, we could not confirm whether this interaction is specific to WTAP. HOTAIR is known to interact with various molecular targets,[25] such as *FTO*, *ALKBH5*, and *YTHDF1*, as predicted by an online database, RBPsuite.[51] Furthermore, HOTAIR can also physically interact with *FTO* and disrupt its ubiquitination and degradation,[52] a potential regulatory mechanism warranting further investigation in PCO.

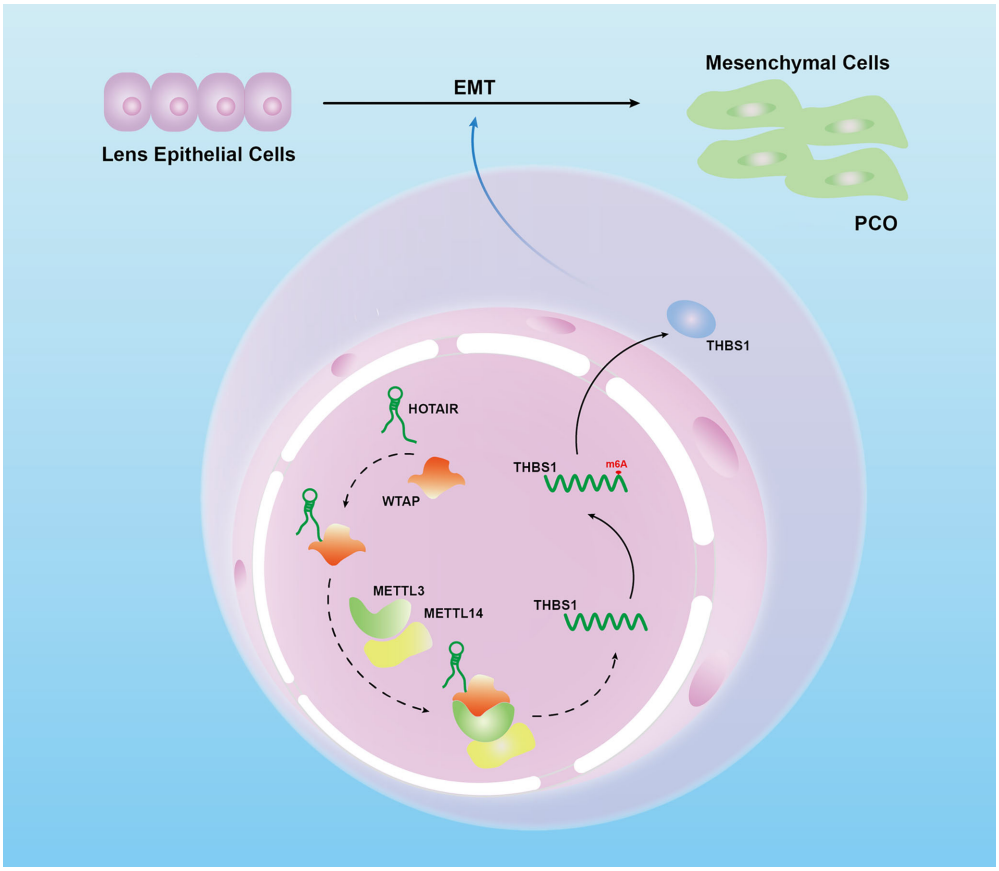


**Figure 12.** The mechanistic scheme of this study. lncRNA HOTAIR/WTAP/THBS1 axis regulates EMT of LECs in PCO.

THBS1, a pro-EMT angiogenesis inhibitor,[53] exacerbates fibrosis and EMT, thereby promoting tumor migration and invasion[54]; however, it also serves as a tumor suppressor.[55] PCO models showed higher THBS1 expression, whereas THBS1 knockdown reduced the EMT intensification caused by HOTAIR overexpression. THBS1 is associated with lens opacity and myopia,[56,57] contributing to PCO formation. Our findings indicate that HOTAIR/WTAP-induced m$^6$A modification stabilizes *THBS1* mRNA, thereby enhancing EMT in LECs. Consistent with previous studies,[28,58] the present study shows that WTAP interacts with THBS1 in an m$^6$A-dependent manner rather than through direct protein–RNA interactions. METTL3-mediated m$^6$A modification is known to increase mRNA stability and gene expression.[59] m$^6$A reader proteins detect the writer-added methylation marks[60] to either degrade[61] or stabilize target mRNAs and promote translation.[50] Moreover, the m$^6$A reader YTHDF1 enhances the stability of *THBS1* mRNA, whereas YTHDF2 recognizes and degrades *THBS1*.[62,63] These findings suggest that YTHDF1/2 may regulate m$^6$A modification and expression level of *THBS1* mediated by the HOTAIR/WTAP complex; however, further studies are warranted to confirm these speculations. Additionally, the specific signaling pathways through which THBS1 regulates EMT in LECs remain unclear. It has been shown that THBS1 mediates cell proliferation, apoptosis, and EMT through the TGF-$\beta$/Smad, Wnt/$\beta$-catenin, and PI3K/Akt signaling pathways.[64–67] Our previous studies confirmed that both the TGF-$\beta$/Smad and canonical Wnt/$\beta$-catenin pathways play a significant role in the EMT of LECs in PCO.[31,32,68] Nevertheless, further studies are needed to investigate the potential regulatory role of THBS1 in these signaling pathways through multiomics approaches.

This study shows that lncRNA HOTAIR, total m$^6$A, and m$^6$A methylase are upregulated in PCO models. HOTAIR binds to WTAP, forming the WTAP/METTL3/METTL14 complex, which enhances THBS1 expression via m$^6$A-dependent mRNA stabilization and promotes EMT in LECs (Fig. 12). These findings suggest that intraocular injection of antisense oligonucleotides and specific compounds inhibiting HOTAIR/WTAP complex formation, or siRNAs targeting THBS1, may effectively inhibit the proliferation, migration, and EMT of LECs, potentially contributing to the prevention and treatment of PCO. These interventions may provide long-term therapeutic benefits by implanting electrospun poly(lactic-co-glycolic) acid (PLGA)-based microtubes equipped with DNA origami nanostructures or long-acting nanomedicine via the integration of an intraocular lens, as demonstrated in our previous studies.[59–61]

In conclusion, this study provides insights into PCO pathogenesis and suggests potential prevention and therapeutic strategies. Investigation into the role of $N^6$-methyladenosine in lens development and the reversal of LEC EMT during PCO formation would be of significant scientific merit.

## *Acknowledgments*

Supported by grants from the National Natural Science Foundation of China (82201165, 82070947), Science and Technology

Program of Xi'an, China (23YXYJ0034), and Health Commission of Xi'an, Shaanxi, China (2023qn09).

Disclosure: **X. Chen**, None; **C. Li**, None; **J. Li**, None; **Z. Guo**, None; **S. Zhang**, None; **C. Guo**, None; **H. Yan**, None

## *References*

1. Liu YC, Wilkins M, Kim T, Malyugin B, Mehta J. Cataracts. *Lancet*. 2017;390(10094):600–612.
2. Konopinska J, Mlynarczyk M, Dmuchowska DA, Obuchowska I. Posterior capsule opacification: a review of experimental studies. *J Clin Med*. 2021;10(13):2847.
3. Milazzo S, Grenot M, Benzerroug M. Posterior capsule opacification. *J Fr Ophtalmol*. 2014;37(10):825–830.
4. Sen P, Kshetrapal M, Shah C, Mohan A, Jain E, Sen A. Posterior capsule opacification rate after phacoemulsification in pediatric cataract: hydrophilic versus hydrophobic intraocular lenses. *J Cataract Refract Surg*. 2019;45(10):1380–1385.
5. Cinar E, Yuce B, Aslan F, Erbakan G. Influence of Nd:YAG laser capsulotomy on toric intraocular lens rotation and change in cylinder power. *J Cataract Refract Surg*. 2024;50(1):43–50.
6. Wang JD, Zhang JS, Li XX, et al. Knockout of TGF-$\beta$ receptor II by CRISPR/Cas9 delays mesenchymal transition of lens epithelium and posterior capsule opacification. *Int J Biol Macromol*. 2024;259(pt 2):129290.
7. Li C, Yan W, Yan H. Oxidative stress, glutaredoxins, and their therapeutic potential in posterior capsular opacification. *Antioxidants*. 2024;13(10):1210.
8. Wormstone IM, Wormstone YM, Smith AJO, Eldred JA. Posterior capsule opacification: what's in the bag? *Prog Retin Eye Res*. 2021;82:100905.
9. Wei CM, Gershowitz A, Moss B. Methylated nucleotides block 5' terminus of HeLa cell messenger RNA. *Cell*. 1975;4(4):379–386.
10. Ma S, Chen C, Ji X, et al. The interplay between m$^{6a}$ RNA methylation and noncoding RNA in cancer. *J Hematol Oncol*. 2019;12(1):121.
11. Wang T, Kong S, Tao M, Ju S. The potential role of RNA N6-methyladenosine in cancer progression. *Mol Cancer*. 2020;19(1):88.
12. Ping XL, Sun BF, Wang L, et al. Mammalian WTAP is a regulatory subunit of the RNA N6-methyladenosine methyltransferase. *Cell Res*. 2014;24(2):177–189.
13. Yang Y, Hsu PJ, Chen YS, Yang Y-G. Dynamic transcriptomic m$^6$A decoration: writers, erasers, readers and functions in RNA metabolism. *Cell Res*. 2018;28(6):616–624.
14. Yue B, Song C, Yang L, et al. METTL3-mediated N6-methyladenosine modification is critical for epithelial-mesenchymal transition and metastasis of gastric cancer. *Mol Cancer*. 2019;18(1):142.
15. Song C, Zhou C. HOXA10 mediates epithelial-mesenchymal transition to promote gastric cancer metastasis partly via modulation of TGFB2/Smad/METTL3 signaling axis. *J Exp Clin Cancer Res*. 2021;40(1):62.
16. Bridges MC, Daulagala AC, Kourtidis A. LNCcation: lncRNA localization and function. *J Cell Biol*. 2021;220(2):e202009045.
17. Yan B, Tao ZF, Li XM, Zhang H, Yao J, Jiang Q. Aberrant expression of long noncoding RNAs in early diabetic retinopathy. *Invest Ophthalmol Vis Sci*. 2014;55(2):941–951.
18. Khan SY, Hackett SF, Riazuddin SA. Non-coding RNA profiling of the developing murine lens. *Exp Eye Res*. 2016;145:347–351.
19. Wang Y, Li P, Wang C, et al. Lens epithelium cell ferroptosis mediated by m$^6$A-lncRNA and GPX4 expression in lens tissue of age-related cataract. *BMC Ophthalmol*. 2023;23(1):514.
20. Shen Y, Dong LF, Zhou RM, et al. Role of long non-coding RNA MIAT in proliferation, apoptosis and migration of lens epithelial cells: A clinical and in vitro study. *J Cell Mol Med*. 2016;20(3):537–548.
21. Xiong L, Sun Y, Huang J, et al. Long non-coding RNA *H19* prevents lens fibrosis through maintaining lens epithelial cell phenotypes. *Cells*. 2022;11(16):2559.
22. Peng C, Wang Y, Ji L, et al. LncRNA-MALAT1/miRNA-204-5p/smad4 axis regulates epithelial-mesenchymal transition, proliferation and migration of lens epithelial cells. *Curr Eye Res*. 2021;46(8):1137–1147.
23. Wang Y, Chen L, Gu Y, et al. LncRNA FEZF1-As1 promotes TGF-$\beta$2-mediated proliferation and migration in human lens epithelial cells SRA01/04. *J Ophthalmol*. 2019;2019:4736203.
24. Dong N. Long noncoding RNA NEAT1 regulates TGF-$\beta$2-induced epithelial-mesenchymal transition of lens epithelial cells through the miR-34a/Snail1 and miR-204/ZEB1 pathways. *Biomed Res Int*. 2020;2020:8352579.
25. Raju GSR, Pavitra E, Bandaru SS, et al. HOTAIR: a potential metastatic, drug-resistant and prognostic regulator of breast cancer. *Mol Cancer*. 2023;22(1):65.
26. Abba MC, Fabre ML, Lee J, Tatineni P, Kil H, Aldaz CM. HOTAIR modulated pathways in early-stage breast cancer progression. *Front Oncol*. 2021;11:783211.
27. Zhang Z, Zhu H, Liu Y, Quan F, Zhang X, Yu L. LncRNA HOTAIR mediates TGF-$\beta$2-induced cell growth and epithelial-mesenchymal transition in human lens epithelial cells. *Acta Biochim Biophys Sin (Shanghai)*. 2018;50(10):1028–1037.
28. Wei W, Sun J, Zhang H, et al. *Circ0008399* interaction with WTAP promotes assembly and activity of the m$^6$A methyltransferase complex and promotes cisplatin resistance in bladder cancer. *Cancer Res*. 2021;81(24):6142–6156.
29. Ding L, Wang R, Zheng Q, et al. CircPDE5A regulates prostate cancer metastasis via controlling WTAP-dependent N6-methyladenisine methylation of EIF3C mRNA. *J Exp Clin Cancer Res*. 2022;41(1):187.
30. Weng L, Qiu K, Gao W, Shi C, Shu F. LncRNA PCGEM1 accelerates non-small cell lung cancer progression via sponging miR-433-3p to upregulate WTAP. *BMC Pulm Med*. 2020;20(1):213.
31. Chen X, Chen Y, Li C, et al. Glutaredoxin 2 protects lens epithelial cells from epithelial-mesenchymal transition by suppressing mitochondrial oxidative stress-related upregulation of integrin-linked kinase. *Exp Eye Res*. 2023;234:109609.
32. Li C, Chen X, Zhang S, et al. Glutaredoxin 1 protects lens epithelial cells from epithelial-mesenchymal transition by preventing casein kinase 1$\alpha$ S-glutathionylation during posterior capsular opacification. *Redox Biol*. 2023;62:102676.
33. Clayton JA, Collins FS. Policy: NIH to balance sex in cell and animal studies. *Nature*. 2014;509(7500):282–283.
34. Wormstone IM, Tamiya S, Eldred JA, et al. Characterisation of TGF-$\beta$2 signalling and function in a human lens cell line. *Exp Eye Res*. 2004;78(3):705–714.
35. Jiao C, Li L, Zhang P, et al. REG$\gamma$ ablation impedes dedifferentiation of anaplastic thyroid carcinoma and accentuates radio-therapeutic response by regulating the Smad7-TGF-$\beta$ pathway. *Cell Death Differ*. 2020;27(2):497–508.
36. Xu QC, Tien YC, Shi YH, et al. METTL3 promotes intrahepatic cholangiocarcinoma progression by regulating IFIT2 expression in an m$^6$A-YTHDF2-dependent manner. *Oncogene*. 2022;41(11):1622–1633.

37. Yao Z-T, Yang Y-M, Sun M-M, et al. New insights into the interplay between long non-coding RNAs and RNA-binding proteins in cancer. *Cancer Commun (Lond)*. 2022; 42(2):117–140.
38. Hentze MW, Castello A, Schwarzl T, Preiss T. A brave new world of RNA-binding proteins. *Nat Rev Mol Cell Biol*. 2018;19(5):327–341.
39. Luo Y, Zhang Y, Pang S, et al. PCBP1 protects bladder cancer cells from mitochondria injury and ferroptosis by inducing LACTB mRNA degradation. *Mol Carcinog*. 2023;62(7):907–919.
40. Li X, Ma B, Zhang W, et al. The essential role of N6-methyladenosine RNA methylation in complex eye diseases. *Genes Dis*. 2023;10(2):505–520.
41. Li P, Yu H, Zhang G, et al. Identification and characterization of N6-methyladenosine circRNAs and methyltransferases in the lens epithelium cells from age-related cataract. *Invest Ophthalmol Vis Sci*. 2020;61(10):13.
42. Yang J, Liu J, Zhao S, Tian F. $N^6$-methyladenosine METTL3 modulates the proliferation and apoptosis of lens epithelial cells in diabetic cataract. *Mol Ther Nucleic Acids*. 2020;20:111–116.
43. Wen K, Zhang Y, Li Y, Wang Q, Sun J. Comprehensive analysis of transcriptome-wide m$^6$A methylome in the anterior capsule of the lens of high myopia patients. *Epigenetics*. 2021;16(9):955–968.
44. Guo M, Su F, Chen Y, Su B. Methyltransferase METTL3-mediated maturation of miR-4654 facilitates high glucose-induced apoptosis and oxidative stress in lens epithelial cells via decreasing SOD2. *Chem Biol Drug Des*. 2024;103(2):e14491.
45. Porman AM, Roberts JT, Duncan ED, et al. A single N6-methyladenosine site regulates lncRNA HOTAIR function in breast cancer cells. *PLoS Biol*. 2022;20(11):e3001885.
46. Liu Q, Yang G-H, Wang N-Z, et al. Dexmedetomidine suppressed the biological behavior of RAW264.7 cells treated with LPS by down-regulating HOTAIR. *Heliyon*. 2024;10(6):e27690.
47. Scholler E, Weichmann F, Treiber T, et al. Interactions, localization, and phosphorylation of the m$^6$A generating METTL3-METTL14-WTAP complex. *RNA*. 2018;24(4):499–512.
48. Hu C, Yu M, Li C, et al. miR-550-1 functions as a tumor suppressor in acute myeloid leukemia via the HIPPO signaling pathway. *Int J Biol Sci*. 2020;16(15):2853–2867.
49. Li B, Zhu L, Lu C, et al. CircNDUFB2 inhibits non-small cell lung cancer progression via destabilizing IGF2BPS and activating anti-tumor immunity. *Nat Commun*. 2021;12(1):295.
50. Wang Y, Lu J-H, Wu Q-N, et al. LncRNA LINRIS stabilizes IGF2BP2 and promotes the aerobic glycolysis in colorectal cancer. *Mol Cancer*. 2019;18(1):174.
51. Pan X, Fang Y, Liu X, Guo X, Shen H-B. RBPsuite 2.0: an updated RNA-protein binding site prediction suite with high coverage on species and proteins based on deep learning. *BMC Biol*. 2025;23(1):74.
52. Wu XM, Mai YX, Wen YF, et al. Silence of HOTAIR promotes osteogenic differentiation and accelerates distraction osteogenesis by mediating FTO ubiquitination. *J Orthop Translat*. 2025;50:248–256.
53. Choi SH, Tamura K, Khajuria RK, et al. Antiangiogenic variant of TSP-1 targets tumor cells in glioblastomas. *Mol Ther*. 2015;23(2):235–243.
54. Tuoheti K, Bai X, Yang L, et al. Forsythiaside a suppresses renal fibrosis and partial epithelial-mesenchymal transition by targeting THBS1 through the PI3K/Akt signaling pathway. *Int Immunopharmacol*. 2024;129:111650.
55. Yang HD, Kim HS, Kim SY, et al. HDAC6 suppresses let-7i-5p to elicit TSP1/CD47-mediated anti-tumorigenesis and phagocytosis of hepatocellular carcinoma. *Hepatology*. 2019;70(4):1262–1279.
56. Nagaya M, Kanada F, Takashima M, Takamura Y, Inatani M, Oki M. Atm inhibition decreases lens opacity in a rat model of galactose-induced cataract. *PLoS One*. 2022;17(9):e0274735.
57. Chen J, Ikeda SI, Yang Y, et al. Scleral remodeling during myopia development in mice eyes: a potential role of thrombospondin-1. *Mol Med*. 2024;30(1):25.
58. Li L-N, Wu J-M, Zheng Z-J, Li S-X, Cai M-Y, Zou M-C. N6-methyladenosine modification of THBS1 induced by affluent WTAP promotes Graves' ophthalmopathy progression through glycolysis to affect Th17/Treg balance. *Autoimmunity*. 2025;58(1):2433628.
59. Li T, Hu PS, Zuo Z, et al. METTL3 facilitates tumor progression via an m$^6$A-IGF2BP2-dependent mechanism in colorectal carcinoma. *Mol Cancer*. 2019;18(1):112.
60. Panneerdoss S, Eedunuri VK, Yadav P, et al. Cross-talk among writers, readers, and erasers of m$^6$A regulates cancer growth and progression. *Sci Adv*. 2018;4(10):eaar8263.
61. Wang X, Lu Z, Gomez A, et al. N6-methyladenosine-dependent regulation of messenger RNA stability. *Nature*. 2014;505(7481):117–120.
62. Shi D, Liu X, Li X, Li T, Liu J, Wu L. YTH m$^6$A RNA-binding protein 1 regulates osteogenesis of MC3T3-E1 cells under hypoxia via translational control of thrombospondin-1. *Int J Mol Sci*. 2023;24(2).
63. Wang Y, Chen J, Gao WQ, Yang R. METTL14 promotes prostate tumorigenesis by inhibiting THBS1 via an m$^6$A-YTHDF2-dependent mechanism. *Cell Death Discov*. 2022;8(1):143.
64. Wen Z, Zhang Y, Wang X, et al. *THBS1*-mediated degradation of collagen via the PI3K/Akt pathway facilitates the metastasis and poor prognosis of OSCC. *Int J Mol Sci*. 2023;24(17):13312.
65. Singh V, Singh AP, Sharma I, et al. Epigenetic deregulations of Wnt/$\beta$-catenin and transforming growth factor beta-Smad pathways in esophageal cancer: outcome of DNA methylation. *J Cancer Res Ther*. 2019;15(1):192–203.
66. Chen L, Fang W, Chen W, et al. Deciphering the molecular mechanism of the *THBS1* gene in the TNF signaling axis in glioma stem cells. *Cell Signal*. 2023;106:110656.
67. Li R, Zhang F, Wang L, et al. Mechanism of THBS1 regulation of MDCK cell proliferation and apoptosis through TGF-$\beta$/Smad signalling. *Int J Mol Sci*. 2025;26(1):395.
68. Chen X, Yan H, Chen Y, Li G, Bin Y, Zhou X. Moderate oxidative stress promotes epithelial-mesenchymal transition in the lens epithelial cells via the TGF-$\beta$/Smad and Wnt/$\beta$-catenin pathways. *Mol Cell Biochem*. 2021;476(3):1631–1642.


Investigative Ophthalmology & Visual Science